Pronounced Effects of Interannular Trimethylene Bridges on the Intramolecular Electron-Transfer Rate in Mixed-Valence Biferrocenium Salts: Valence-Trapped Electronic Structure with Unusual Structural and Mössbauer Characteristics

Teng-Yuan Dong,[*,1] Ting-Yu Lee,[1a] Shu-Hwei Lee,[1b] Gene-Hsiang Lee,[2] and Shie-Ming Peng[2]

Department of Chemistry, National Sun Yat-sen University, Kaohsuing, Taiwan, ROC, the Institute of Chemistry, Academia Sinica, Nankang, Taipei, Taiwan, ROC, and Department of Chemistry, National Taiwan University, Taipei, Taiwan, ROC

The X-ray structure determinations of two new constitutional isomers of mixed-valence biferrocenium salts and the effects of interannular trimethylene bridges on intramolecular electron-transfer rates in both solid and solution states are reported. The X-ray structure of $1',2:3',4:1''',2'':3''',4''$-tetrakis(propane-1,3-diyl)-$1,1''$-biferrocene (**17a**) has been determined at 298 K: $P\bar{1}$, $a = 9.144(1)$ Å, $b = 15.051(2)$ Å, $c = 17.844(4)$ Å, $\alpha = 106.39(3)°$, $\beta = 91.73(2)°$, $\gamma = 90.76(2)°$, $Z = 4$, $D_c = 1.496$ g cm^{-3}, $R_F = 0.040$, and $R_{wF} = 0.046$. The isomeric compound **17b** crystallizes in the triclinic space group $P\bar{1}$ with eight molecules in a unit cell with dimensions $a = 9.209(1)$ Å, $b = 24.132(2)$ Å, $c = 24.501(4)$ Å, $\alpha = 116.808(9)°$, $\beta = 87.98(1)°$, $\gamma = 91.58(1)°$, $D_c = 1.451$ g cm^{-3}, $R_F = 0.038$, and $R_{wF} = 0.041$. The mixed-valence compound $1',2:3',4:1''',2'':3''',4''$-tetrakis(propane-1,3-diyl)-$1,1''$-biferrocenium triiodide (**18a**) crystallizes in the monoclinic space group $P2_1/c$ with $a = 11.363(2)$ Å, $b = 13.666(2)$ Å, $c = 19.753(3)$ Å, $\beta = 104.793(12)°$, $Z = 4$, $D_c = 2.04$ g cm^{-3}, $R_F = 0.039$, and $R_{wF} = 0.043$. The isomeric mixed-valence compound **18b** crystallizes in the monoclinic space group $P2_1/n$ with $a = 11.578(1)$ Å, $b = 12.108(2)$ Å, $c = 21.162(3)$ Å, $\beta = 90.379°$, $Z = 4$, $D_c = 2.04$ g cm^{-3}, $R_F = 0.030$, and $R_{wF} = 0.032$. In common with most mixed-valence compounds, compounds **18a** and **18b** in CH$_2$Cl$_2$ have intervalence transition (IT) bands at 5050 and 4808 cm^{-1}, respectively. The corresponding rate constants of intramolecular electron-transfer rates for **18a,b** are 2.31×10^{12} and 3.26×10^{12} s^{-1}, respectively. The Mössbauer results indicate that compounds **18a,b** have valence-trapped electronic structures (electron-transfer rate less than $\sim 10^7$ s^{-1} in solid state). We believe that the most important factor controlling the difference of intramolecular electron-transfer rates between the solution state and the solid state is the degree of coplanarity between the two Cp rings in the fulvalenide bridge. We also demonstrate that the perturbations caused by the interannular trimethylene bridge have dramatic influences on the electronic structure in a series of model ferrocenium salts.

Introduction

There has been considerable progress made in understanding the factors which control the rate of intramolecular electron transfer in the solid state for mixed-valence compounds.[3] The rates of electron transfer in mixed-valence cations 1–13 (Chart 1) can be sensitively controlled by environmental factors.[4-24] Compounds 2–5 give unusual temperature-dependent Mössbauer spectra.[5-8] At temperatures below 200 K they show two doublets, one for the Fe^{II} and the other for the Fe^{III} sites. Increasing the sample temperature in each case causes the two doublets to move

(9) Nakashima, S.; Masuda, Y.; Motoyama, I.; Sano, H. *Bull. Chem. Soc. Jpn.* **1987**, *60*, 1673.

(10) Nakashima, S.; Katada, M.; Motoyama, I.; Sano, H. *Bull. Chem. Soc. Jpn.* **1987**, *60*, 2253.

(11) Dong, T.-Y.; Kambara, T.; Hendrickson, D. N. *J. Am. Chem. Soc.* **1986**, *108*, 4423.

(12) Dong, T.-Y.; Kambara, T.; Hendrickson, D. N. *J. Am. Chem. Soc.* **1986**, *108*, 5857.

(13) Sorai, M.; Nishimori, A.; Hendrickson, D. N.; Dong, T.-Y.; Cohn, M. J. *J. Am. Chem. Soc.* **1987**, *109*, 4266.

(14) Kambara, T.; Hendrickson, D. N.; Dong, T.-Y.; Cohn, M. J. *J. Chem. Phys.* **1987**, *86*, 2326.

(15) Konno, M.; Hyodo, S.; Iijima, S. *Bull. Chem. Soc. Jpn.* **1982**, *55*, 2327.

(16) Wong, K. Y.; Schatz, P. N. *Prog. Inorg. Chem.* **1981**, *28*, 369.

(17) Dong, T.-Y.; Hwang, M. Y.; Schei, C. C.; Peng, S. M.; Yeh, S. K. *J. Organomet. Chem.* **1989**, *369*, C33.

(18) Dong, T.-Y.; Schei, C. C.; Hwang, M. Y.; Lee, T. Y.; Yeh, S. K.; Wen, Y. S. *Organometallics* **1992**, *11*, 573.
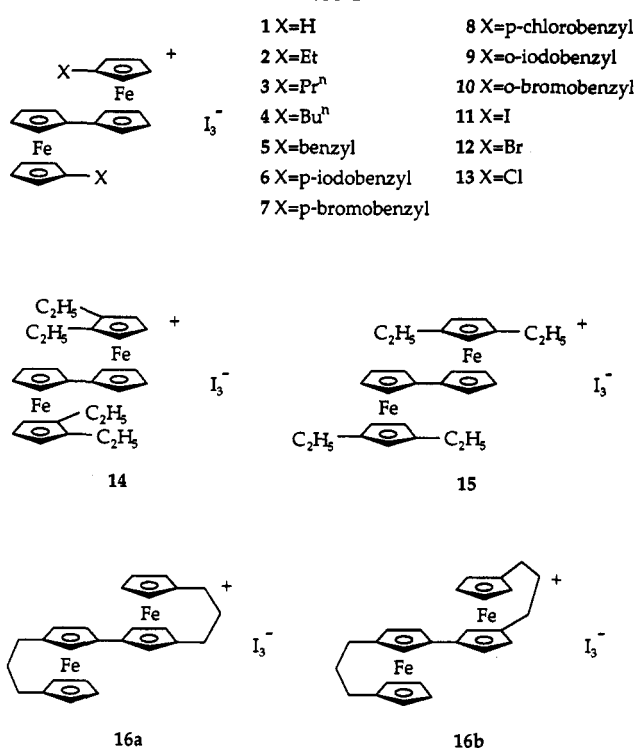
(19) Kai, M.; Katada, M.; Sano, H. *Chem. Lett.* **1988**, 1523.

(20) Dong, T.-Y.; Schei, C. C.; Hsu, T. L.; Lee, S. L.; Li, S. J. *Inorg. Chem.* **1991**, *30*, 2457.

(21) Dong, T.-Y.; Chou, C. Y. *J. Chem. Soc., Chem. Commun.* **1990**, 1332.

(22) Webb, R. J.; Geib, S. J.; Staley, D. L.; Rheingold, A. L.; Hendrickson, D. N. *J. Am. Chem. Soc.* **1990**, *112*, 5031.

[⊛] Abstract published in *Advance ACS Abstracts*, April 15, 1994.

(1) (a) Academia Sinica. (b) National Sun Yat-sen University.

(2) National Taiwan University.

(3) For reviews, see: (a) Day, P. *Int. Rev. Phys. Chem.* **1981**, *1*, 149. (b) Brown, D. B., Ed. *Mixed-Valence Compounds, Theory and Applications in Chemistry, Physics, Geology, and Biology*; Reidel: Boston, MA, 1980. (c) Creutz, C. *Prog. Inorg. Chem.* **1983**, *30*, 1–73. (d) Richardson, D. E.; Taube, H. *Coord. Chem. Rev.* **1984**, *60*, 107.

(4) Hendrickson, D. N.; Oh, S. M.; Dong, T.-Y.; Moore, M. F. *Comments Inorg. Chem.* **1985**, *4*, 329.

(5) Dong, T.-Y.; Cohn, M. J.; Hendrickson, D. N.; Pierpont, C. G. *J. Am. Chem. Soc.* **1985**, *107*, 4777.

(6) Cohn, M. J.; Dong, T.-Y.; Hendrickson, D. N.; Geib, S. J.; Rheingold, A. L. *J. Chem. Soc., Chem. Commun.* **1985**, 1095.

(7) Dong, T.-Y.; Hendrickson, D. N.; Iwai, K.; Cohn, M. J.; Rheingold, A. L.; Sano, H.; Motoyama, S. *J. Am. Chem. Soc.* **1985**, *107*, 7996.

(8) Iijima, S.; Saida, R.; Motoyama, I.; Sano, H. *Bull. Chem. Soc. Jpn.* **1981**, *54*, 1375.

Chart 1

1 X=H	8 X=p-chlorobenzyl
2 X=Et	9 X=o-iodobenzyl
3 X=Pr^n	10 X=o-bromobenzyl
4 X=Bu^n	11 X=I
5 X=benzyl	12 X=Br
6 X=p-iodobenzyl	13 X=Cl
7 X=p-bromobenzyl	

14 15

16a 16b

Scheme 1

17a 17b

18a 18b

together with no discernible line broadening and eventually to become a single "average-valence" doublet at temperatures of 275, 245, 275, and 260 K, respectively. Hendrickson suggested[4] that the nature of the solid-state environment about a mixed-valence biferrocenium cation can have a dramatic impact on the rate of electron transfer. When there is an onset of dynamics associated with the counterions, or ligands, this will probably influence the rate of intramolecular electron transfer. Very recently, we found that changing the substituent in the benzyl unit in compounds 6–10 leads to dramatic changes in the electron-transfer rate in the solid state.[17,18] The features in the variable-temperature (77–300 K) ^{57}Fe Mössbauer spectra of 6 and 8 include two doublets, which are expected for a mixed-valence cation localized on the time scale of the Mössbauer technique (electron-transfer rates less than $\sim 10^7$ s^{-1}). In the case of 7, at temperatures below 150 K, two doublets are observed in the Mössbauer spectra, and increasing the temperature causes two doublets to become a single average-valence doublet at a temperature of ~ 200 K. In comparison with compounds 6–8, a single average-valence doublet is seen even at 77 K for 9 and 10. We suggested[18] that the interactions between the cation and anion undoubtedly alter the potential energy surface of the mixed-valence molecule and, therefore, the rate of intramolecular electron transfer.

A recent interesting finding is that there is a significant influence on the electron-transfer rate in the mixed-valence biferrocenium salt when the cyclopentadienyl (Cp) rings in each ferrocenyl moiety are tilted from a parallel geometry.[21,24–26] Such a structural modification of the parallel relation between the two Cp rings around the Fe
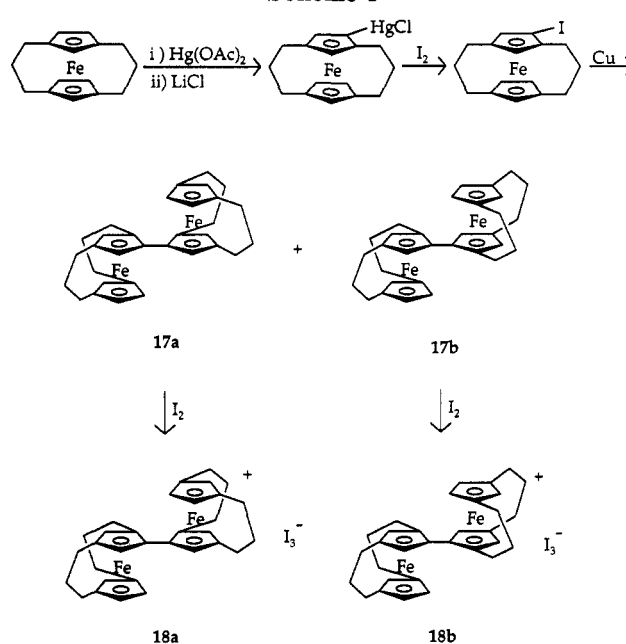
Table 1. Experimental and Crystal Data for the X-ray Structures

	17a	17b	18a	18b
formula	C$_{32}$H$_{34}$Fe$_2$	C$_{32}$H$_{34}$Fe$_2$	C$_{32}$H$_{34}$Fe$_2$I$_3$	C$_{32}$H$_{34}$Fe$_2$I$_3$
mw	530.31	530.31	911.02	911.02
cryst syst	triclinic	triclinic	monoclinic	monoclinic
space group	P$\bar{1}$	P$\bar{1}$	P2$_1$/c	P2$_1$/n
a, Å	9.144(1)	9.209(1)	11.363(2)	11.578(1)
b, Å	15.051(2)	24.132(2)	13.666(2)	12.108(2)
c, Å	17.844(4)	24.501(4)	19.753(3)	21.162(3)
α, deg	106.39(3)	116.808(9)		
β, deg	91.73(2)	87.98(1)	104.79(1)	90.379(8)
γ, deg	90.76(2)	91.58(1)		
V, Å^3	2354.3(7)	4856.2(1)	2965.6(7)	2966.5(7)
Z	4	8	4	4
D$_{calcd}$, g cm^{-3}	1.496	1.451	2.040	2.040
μ, mm^{-1}	1.25	1.21	4.09	4.09
λ, Å	0.709 30	0.709 30	0.709 30	0.709 30
2θ limits, deg	44.9	44.8	44.9	49.8
max, min transmissn coeff	0.996, 0.926	0.999, 0.939	0.998, 0.601	0.999, 0.781
R$_F$	0.040	0.038	0.039	0.030
R$_{wF}$	0.046	0.041	0.043	0.032

ion would lead to greater metal–ligand interactions as the rings tilt. Compounds 14–16 are of use in understanding the influence of tilted Cp rings on the rate of electron transfer.[25,26] Compounds 14 and 15 are delocalized on the Mössbauer time scale in the solid state above 195 and 125 K, respectively. We suggested[26] that the difference in electron transfer rates for the series of dialkylbiferrocenium cations is mainly due to the degree of tilting of the Cp rings from the parallel geometry. Deviations of the Cp rings from the parallel position were found to correlate quite well with the critical temperature of electronic delocalization–localization in mixed-valence biferrocenium salts. In the case of 16, there is a significant influence on the electron-transfer rate when the Cp rings in the ferrocenyl moieties are linked by an interannular trimethylene bridge.[21,24] The Mössbauer results indicate that compound 16 is delocalized on the Mössbauer time scale above 77 K. Only a single average-valence doublet (ΔE_Q

(23) Webb, R. J.; Rheingold, A. L.; Geib, S. J.; Staley, D. L.; Hendrickson, D. N. *Angew. Chem., Int. Ed. Engl.* **1989**, 28, 1388.

(24) Dong, T.-Y.; Lee, T. Y.; Lin, H. M. *J. Organomet. Chem.* **1992**, 427.

(25) Dong, T.-Y.; Chang, C. K.; Huang, C. H.; Wen, Y. S.; Lee, S. L.; Chen, J. A.; Yeh, W. Y.; Yeh, A. *J. Chem. Soc., Chem. Commun.* **1992**, 526.

(26) Dong, T.-Y.; Huang, C. H.; Chang, C. K.; Wen, Y. S.; Lee, S. L.; Chen, J. A.; Yeh, W. Y.; Yeh, A. *J. Am. Chem. Soc.* **1993**, 115, 6357.

Table 2. Atom Coordinates and Thermal Parameters ($Å^2$) for 17a

	x	y	z	$B_{iso}{}^a$		x	y	z	$B_{iso}{}^a$
Fe1A	0.76986(8)	0.01167(5)	0.16510(4)	2.66(3)	C31A	0.8280(6)	−0.4011(4)	0.0828(3)	3.9(3)
Fe1B	0.27004(8)	0.49640(5)	0.32340(4)	2.34(3)	C32A	0.8405(6)	−0.3686(4)	0.0098(3)	4.1(3)
Fe2A	0.56661(8)	−0.26275(5)	0.06193(4)	2.26(3)	C1B	0.1835(5)	0.6047(3)	0.2900(3)	2.4(2)
Fe2B	0.05500(8)	0.75840(5)	0.43502(4)	2.66(3)	C2B	0.1551(5)	0.5161(3)	0.2325(3)	2.4(2)
C1A	0.7487(6)	−0.1099(3)	0.1924(3)	2.6(2)	C3B	0.2937(6)	0.4771(3)	0.2086(3)	2.7(2)
C2A	0.7514(6)	−0.0312(3)	0.2607(3)	3.1(2)	C4B	0.4067(5)	0.5364(3)	0.2530(3)	2.8(2)
C3A	0.8870(6)	0.0172(4)	0.2629(3)	3.6(3)	C5B	0.3375(6)	0.6152(3)	0.3020(3)	2.9(3)
C4A	0.9669(5)	−0.0268(3)	0.1947(3)	3.1(3)	C6B	0.1490(6)	0.4000(3)	0.3502(3)	3.0(2)
C5A	0.8815(6)	−0.1066(3)	0.1534(3)	2.9(2)	C7B	0.2862(6)	0.3639(3)	0.3230(3)	3.0(2)
C6A	0.6081(6)	0.1026(4)	0.1777(3)	3.9(3)	C8B	0.3996(6)	0.4190(4)	0.3707(3)	3.5(3)
C7A	0.7476(6)	0.1483(4)	0.1804(3)	4.0(3)	C9B	0.3320(6)	0.4865(4)	0.4312(3)	3.5(3)
C8A	0.8238(6)	0.1070(3)	0.1109(3)	3.7(3)	C10B	0.1771(6)	0.4745(4)	0.4190(3)	3.4(3)
C9A	0.7258(6)	0.0392(4)	0.0615(3)	3.8(3)	C11B	0.0708(5)	0.6714(3)	0.3259(3)	2.5(2)
C10A	0.5943(6)	0.0365(4)	0.1017(3)	3.8(3)	C12B	−0.0583(6)	0.6514(3)	0.3616(3)	3.0(2)
C11A	0.6347(5)	−0.1825(3)	0.1697(3)	2.7(2)	C13B	−0.1450(6)	0.7315(4)	0.3842(3)	3.4(3)
C12A	0.4816(6)	−0.1720(3)	0.1559(3)	3.1(2)	C14B	−0.0706(6)	0.8010(4)	0.3590(3)	3.4(3)
C13A	0.4095(6)	−0.2594(4)	0.1376(3)	3.2(2)	C15B	0.0649(6)	0.7669(3)	0.3254(3)	3.1(2)
C14A	0.5171(6)	−0.3246(3)	0.1435(3)	3.1(2)	C16B	0.0085(6)	0.8095(4)	0.5473(3)	3.6(3)
C15A	0.6567(6)	−0.2790(3)	0.1608(3)	2.7(2)	C17B	0.0790(6)	0.8780(4)	0.5198(3)	3.6(3)
C16A	0.7044(6)	−0.3313(4)	−0.0172(3)	3.0(3)	C18B	0.2160(6)	0.8455(4)	0.4888(3)	3.8(3)
C17A	0.5654(6)	−0.3763(3)	−0.0297(3)	3.0(2)	C19B	0.2354(7)	0.7568(4)	0.5027(3)	4.3(3)
C18A	0.4582(6)	−0.3129(4)	−0.0414(3)	3.4(3)	C20B	0.1082(7)	0.7356(4)	0.5385(3)	4.1(3)
C19A	0.5337(6)	−0.2302(4)	−0.0400(3)	3.8(3)	C21B	0.0107(6)	0.4666(3)	0.2082(3)	2.8(2)
C20A	0.6838(6)	−0.2412(4)	−0.0258(3)	3.5(3)	C22B	0.0013(6)	0.3706(3)	0.2225(3)	3.3(2)
C21A	0.6248(7)	0.0022(4)	0.3143(3)	4.2(3)	C23B	0.0044(6)	0.3712(4)	0.3087(3)	3.5(3)
C22A	0.5772(7)	0.1011(4)	0.3190(4)	5.5(3)	C24B	0.5655(6)	0.5123(4)	0.2549(3)	3.6(3)
C23A	0.5086(7)	0.1134(4)	0.2441(4)	5.3(3)	C25B	0.5944(6)	0.4187(4)	0.2706(4)	4.8(3)
C24A	1.1016(6)	0.0109(4)	0.1675(4)	4.5(3)	C26B	0.5603(6)	0.4139(4)	0.3532(3)	4.4(3)
C25A	1.0888(6)	0.1098(4)	0.1601(4)	4.5(3)	C27B	−0.2769(7)	0.7452(4)	0.4338(4)	5.1(3)
C26A	0.9807(7)	0.1217(4)	0.0974(4)	4.3(3)	C28B	−0.2572(9)	0.807(1)	0.5118(5)	15.6(9)
C27A	0.2538(6)	−0.2834(4)	0.1070(3)	4.4(3)	C29B	−0.1471(7)	0.8099(4)	0.5713(3)	4.7(3)
C28A	0.2415(7)	−0.3596(5)	0.0303(5)	6.9(4)	C30B	0.1819(7)	0.8250(3)	0.3048(3)	3.8(3)
C29A	0.2960(7)	−0.3266(4)	−0.0423(4)	4.8(3)	C31B	0.2322(7)	0.9096(4)	0.3717(4)	4.6(3)
C30A	0.8013(6)	−0.3262(4)	0.1591(3)	3.6(3)	C32B	0.3111(7)	0.8901(4)	0.4413(4)	4.9(3)

^{a} B_{iso} is the mean of the principal axes of the thermal ellipsoid.

= 1.614 mm s^{-1}) is observed from 77 to 300 K. In our previous papers,[21,24] we proposed that such a structural modification would lead to increased metal–ligand interactions as the rings tilt. However, there is still one important question that remains. At temperatures below 5 K, compound **16** shows two doublets in the ^{57}Fe Mössbauer spectra, one with a quadrupole splitting (ΔE_Q) of ~1.36 mm s^{-1} and the other with ΔE_Q ~1.88 mm s^{-1}.[27] Two possible explanations for this ^{57}Fe Mössbauer spectrum may be taken into account. First, the Mössbauer results indicate that the valence state of iron atoms in compound **16** is localized on the Mössbauer time scale (10^7 s^{-1}) in the solid state at 4.2 K. A second possibility is that the Mössbauer sample contained both constitutional isomers **16a,b** in a 1:1 ratio. Unfortunately, a suitable crystal of **16** for X-ray determination cannot be obtained. To study the effects of interannular bridges, we have prepared the two new constitutional isomers **18a,b** (Scheme 1) and determined the crystal structures of **17a,b** and **18a,b**. We now show that there is a dramatic difference in electron-transfer rates between **16** and **18**. Furthermore, the unusual physical properties of **18** are explained in terms of structural characteristics.

Experimental Section

General Information. All manipulations involving air-sensitive materials were carried out by using standard Schlenk techniques under an atmosphere of N_2. Chromatography was performed on neutral alumina (activity II), with hexane/CH_2Cl_2 as eluent. Solvents were purified as follows: benzene, hexane, and ether distilled from Na/benzophenone; CH_2Cl_2, distilled from

P_2O_5. 1,1′:3,3′-Bis(propane-1,3-diyl)ferrocene was prepared according to the literature procedure[28] and identified by its melting point, NMR, and mass spectrum.

Mercuration of 1,1′:3,3′-Bis(propane-1,3-diyl)ferrocene. A CH_3OH (75 mL) solution of mercuric acetate (2.6 g, 8.16 mmol) was added dropwise to a hot solution of 1,1′:3,3′-bis(propane-1,3-diyl)ferrocene (3.5 g, 13.15 mmol) dissolved in 80 mL of absolute CH_3OH and 50 mL of dry ether. The mixture was refluxed for 18 h, and then LiCl (0.5 g) in 65 mL of hot CH_3OH was added dropwise. A yellow precipitate was formed immediately out of an orange solution. The solvent was removed under vacuum. The resulting yellow powder was put into a Soxhlet extractor and extracted with hexane to yield the starting material. Further extraction with CH_2Cl_2 yielded 1.36 g (33%) of a yellow solid. The crude product was used without further purification.

Iodination of Mercurated 1,1′:3,3′-Bis(propane-1,3-diyl)-ferrocene. N-Iodosuccinimide (NIS; 0.78 g, 3.5 mmol) in 75 mL of CH_2Cl_2 was added dropwise at 0 °C to 1.36 g (2.71 mmol) of mercurated 1,1′:3,3′-bis(propane-1,3-diyl)ferrocene. The reaction mixture was warmed to room temperature and was stirred overnight. To this was added 50 mL of 10% aqueous $Na_2S_2O_3$ followed by 50 mL of 10% aqueous $NaHCO_3$. The organic layers were separated, and the aqueous portion was extracted with 3 × 50 mL portions of CH_2Cl_2. The combined organic layer was washed twice with 100 mL of 10% aqueous $NaHCO_3$ and twice with 100 mL of H_2O and dried over $MgSO_4$. The solvent was removed under reduced pressure. The red oily residue was chromatographed, with hexane as eluent. The first band was the desired compound (~0.5 g, 50%). The properties of 4-iodo-1,1′:3,3′-bis(propane-1,3-diyl)ferrocene are as follows: ^{1}H NMR ($CDCl_3$, ppm) 3.5–4.5 (5H, m, ring protons), 1.5–2.5 (12H, m, methylene protons); mass spectrum M$^+$ at m/z 392.

(27) Unpublished results.

(28) Crawford, W.; Turbitt, T. D.; Watts, W. E. *J. Organomet. Chem.* **1976**, *105*, 341.

Table 3. Selected Bond Distances (Å) and Bond Angles (deg)

	17a		18a	18b
	A	B		
I1–I2			2.905(2)	2.9393(6)
I1–I3			2.908(3)	2.9058(7)
Fe1–C1	2.030(5)	2.047(5)	2.042(9)	2.136(5)
Fe1–C2	1.997(5)	2.001(4)	2.02(1)	2.031(5)
Fe1–C3	2.000(5)	2.001(5)	2.03(1)	2.019(5)
Fe1–C4	2.000(5)	2.001(5)	2.01(1)	2.032(5)
Fe1–C5	2.027(5)	2.023(5)	2.02(1)	2.088(5)
Fe1–C6	2.002(5)	1.985(5)	2.02(1)	2.036(5)
Fe1–C7	2.011(5)	2.000(5)	2.00(1)	2.014(5)
Fe1–C8	2.007(5)	2.001(5)	2.00(1)	2.042(5)
Fe1–C9	2.035(5)	2.035(5)	2.03(1)	2.099(5)
Fe1–C10	2.035(5)	2.034(5)	2.02(1)	2.089(5)
Fe2–C11	2.035(5)	2.028(5)	2.099(9)	2.031(5)
Fe2–C12	2.024(5)	2.016(5)	2.06(1)	2.023(5)
Fe2–C13	1.992(5)	2.001(5)	2.02(1)	2.006(5)
Fe2–C14	1.997(5)	1.997(5)	2.02(1)	2.006(5)
Fe2–C15	2.003(5)	2.001(5)	2.05(1)	2.011(5)
Fe2–C16	1.991(5)	1.994(5)	2.05(1)	2.011(5)
Fe2–C17	2.004(5)	2.002(5)	2.07(1)	2.012(5)
Fe2–C18	1.991(5)	1.991(5)	2.08(1)	2.008(5)
Fe2–C19	2.019(6)	2.019(6)	2.06(1)	2.031(5)
Fe2–C20	2.018(5)	2.018(5)	2.05(1)	2.025(5)
C1–C2	1.439(7)	1.449(6)	1.46(2)	1.449(7)
C1–C5	1.424(7)	1.418(7)	1.44(2)	1.436(7)
C1–C11	1.462(7)	1.478(7)	1.44(1)	1.455(7)
C2–C3	1.424(8)	1.428(7)	1.49(2)	1.422(7)
C3–C4	1.437(8)	1.421(7)	1.44(2)	1.424(8)
C4–C5	1.428(7)	1.427(7)	1.43(2)	1.427(7)
C6–C7	1.435(8)	1.418(7)	1.44(2)	1.422(7)
C6–C10	1.438(9)	1.424(7)	1.45(2)	1.425(8)
C7–C8	1.427(8)	1.419(8)	1.41(2)	1.421(8)
C8–C9	1.429(8)	1.420(8)	1.43(2)	1.440(8)
C9–C10	1.425(9)	1.427(8)	1.38(2)	1.404(8)
C11–C12	1.433(7)	1.428(7)	1.46(1)	1.439(7)
C11–C15	1.433(7)	1.441(7)	1.44(1)	1.455(7)
C12–C13	1.411(7)	1.420(7)	1.42(1)	1.421(8)
C13–C14	1.422(8)	1.422(8)	1.41(2)	1.434(8)
C14–C15	1.425(7)	1.431(8)	1.44(2)	1.428(7)
C16–C17	1.413(7)	1.416(8)	1.44(2)	1.429(9)
C16–C20	1.422(7)	1.424(8)	1.45(2)	1.436(9)
C17–C18	1.428(7)	1.421(8)	1.43(2)	1.424(8)
C18–C19	1.409(8)	1.438(8)	1.42(2)	1.425(9)
C19–C20	1.408(8)	1.419(9)	1.39(2)	1.423(9)
I2–I1–I3			177.26(4)	175.65(2)
C2–C1–C5	107.2(4)	107.0(4)	109.1(9)	106.5(4)
C2–C1–C11	126.3(4)	125.3(4)	125(1)	128.4(4)
C5–C1–C11	126.4(4)	127.7(4)	125.5(9)	125.1(4)
C1–C2–C3	107.4(5)	107.3(4)	105(1)	107.3(4)
C2–C3–C4	109.4(4)	109.1(4)	109(1)	109.9(4)
C3–C4–C5	106.0(4)	106.9(4)	108(1)	106.3(4)
C1–C5–C4	109.8(4)	109.6(4)	109(1)	109.7(4)
C7–C6–C10	105.9(5)	107.3(5)	103(1)	105.2(5)
C6–C7–C8	110.0(5)	109.1(4)	110(1)	110.8(5)
C7–C8–C9	106.5(5)	107.3(5)	108(1)	105.7(5)
C8–C9–C10	108.7(5)	108.2(5)	107(1)	108.2(5)
C6–C10–C9	108.7(5)	108.0(5)	111(1)	110.0(5)
C1–C11–C12	127.9(4)	126.3(4)	125.4(9)	128.0(4)
C1–C11–C15	125.2(4)	126.2(4)	126.2(9)	124.3(4)
C12–C11–C15	106.9(4)	107.3(4)	107.9(8)	107.6(4)
C11–C12–C13	109.6(4)	110.0(4)	108.0(8)	109.0(4)
C12–C13–C14	106.7(4)	106.0(5)	107.7(9)	106.9(4)
C13–C14–C15	109.4(4)	110.3(4)	110.3(9)	110.0(4)
C11–C15–C14	107.3(4)	106.4(5)	105.9(9)	106.4(4)
C17–C16–C20	106.6(4)	106.7(5)	106(1)	105.0(5)
C16–C17–C18	109.1(4)	109.8(5)	110(1)	110.8(5)
C17–C18–C19	106.9(5)	106.6(5)	106(1)	106.4(5)
C18–C19–C20	108.6(5)	107.8(5)	111(1)	108.3(5)
C16–C20–C19	108.7(5)	109.0(5)	108(1)	109.4(5)

Neutral Compounds 17a,b. Compounds 17a,b were prepared by the Ullman coupling procedure as shown in Scheme 1. A mixture of 4-iodo-1,1′:3,3′-bis(propane-1,3-diyl)ferrocene (0.5 g) and activated copper (2 g) was heated under N_2 at 110–120 °C for 24 h. After it was cooled to room temperature, the reaction

mixture was repeatedly extracted with CH_2Cl_2 until the CH_2Cl_2 extracts appeared colorless. The extracts were evaporated and chromatographed on neutral Al_2O_3. The first band eluted with hexane yielded the starting material. Continued elution with hexane afforded the desired compounds 17a (0.1 g, second band) and 17b (0.1 g, third band). Compounds 17a,b were recrystallized from benzene/hexane. 17a: ^{1}H NMR ($CDCl_3$, ppm) 4.12 (s, 2H, Cp), 4.07 (s, 2H, Cp), 3.79 (s, 2H, Cp), 3.73 (s, 2H, Cp), 3.59 (s, 2H, Cp), 2.2–1.4 (m, 24H, –CH_2–); mp 242–243 °C; mass spectrum M^+ at m/z 530. 17b: ^{1}H NMR ($CDCl_3$, ppm) 3.99 (s, 4H, Cp), 3.82 (s, 2H, Cp), 3.73 (s, 2H, Cp), 3.47 (s, 2H, Cp), 2.3–1.4 (m, 24H, –CH_2–); mp 192–193 °C; mass spectrum M^+ at m/z 530.

Mixed-Valence Compounds 18a,b. A crystalline sample of 18a was prepared by adding a benzene/hexane (1:1) solution containing a stoichiometric amount of iodine to a benzene/hexane (1:1) solution of the corresponding biferrocene at 0 °C. The resulting dark green crystals were filtered and washed repeatedly with cold hexane. The same method described for the preparation of 18a was used to synthesize 18b, except dry ether was used instead of benzene/hexane. Anal. Calcd for 18a ($C_{32}H_{34}Fe_2I_3$): C, 42.19; H, 3.76. Found: C, 42.03; H, 3.80. Calcd for 18b ($C_{32}H_{34}Fe_2I_3$): C, 42.19; H, 3.76. Found: C, 42.19; H, 3.44.

Physical Methods. ^{57}Fe Mössbauer measurements were made on a constant-velocity instrument which has been previously described.[18] The absolute temperature accuracy is estimated to be ±5 K, while the relative precision is ±0.5 K. Computer fittings of the ^{57}Fe Mössbauer data to Lorentzian lines were carried out with a modified version of a previously reported program.[29] Velocity calibrations were made using a 99.99% pure 10-μm iron foil. Typical line widths for all three pairs of iron lines fell in the range 0.24–0.27 mm/s. Isomer shifts are reported relative to iron foil at 300 K but are uncorrected for temperature-dependent, second-order Doppler effects. It should be noted that the isomer shifts illustrated in the figures are plotted as obtained experimentally. Tabulated data are provided.

^{1}H NMR spectra were recorded on a Bruker AMX500 spectrometer. Mass spectra were obtained with a VG250-70S system. The near-IR spectra were recorded from 2300 to 900 nm in CH_2Cl_2 by using 1.0-cm quartz cells with a Perkin-Elmer Lambda 9 spectrophotometer.

Electrochemical measurements were carried out with a BAS 100B system. Cyclic voltammetry was performed with a stationary glassy-carbon working electrode, which was cleaned after each run. These experiments were carried out with 1 × 10⁻³ M solutions of biferrocene in dry CH_2Cl_2/CH_3CN (1:1) containing 0.1 M of (n-C_4H_9)$_4$NPF$_6$ as supporting electrolyte. The potentials quoted in this work are relative to a Ag/AgCl electrode at 25 °C. Under these conditions, ferrocene shows a reversible one-electron-oxidation wave ($E_{1/2}$ = 0.37 V).

The single-crystal X-ray determinations of compounds 17a,b and 18a,b were carried out on an Enraf-Nonius CAD4 diffractometer at 298 K. Absorption corrections were made with empirical ψ rotation for all four compounds. The X-ray crystal data are summarized in Table 1. Complete tables of bond distances and angles and of thermal parameters for these compounds are given as supplementary material.

Structure Determination of 17a. An orange crystal (0.29 × 0.28 × 0.34 mm), which was grown by slow evaporation from a hexane solution, was used for data collection at 298 K. Cell dimensions were obtained from 20 reflections with 14.95° < 2θ < 29.41°. The θ–2θ scan technique was used to record the intensities for all reflections for which 1° < 2θ < 44.9°. Of the 6139 unique reflections, there were 4458 reflections with F_o > 2.0$\sigma(F_o{}^2)$, where $\sigma(F_o{}^2)$ values were estimated from counting statistics. These data were used in the final refinement of the structural parameters.

A three-dimensional Patterson synthesis was used to determine the heavy-atom positions, which phased the data sufficiently well to permit location of the remaining non-hydrogen atoms from Fourier synthesis. All non-hydrogen atoms were refined

(29) Lee, J. F.; Lee, M. D.; Tseng, P. K. *Chemistry* 1987, *45*, 50.

Table 4. Atom Coordinates and Thermal Parameters (Å²) for 17b

	x	y	z	B_{iso}		x	y	z	B_{iso}
Fe1A	0.3252(1)	0.65726(5)	0.26522(6)	2.91(6)	Fe1C	0.0645(1)	0.16076(5)	0.97554(6)	3.87(7)
Fe2A	0.2686(1)	0.87082(5)	0.28248(5)	3.45(7)	Fe2C	0.3337(1)	0.36133(5)	1.02230(5)	3.35(7)
C1A	0.3714(8)	0.7351(3)	0.2543(3)	2.6(4)	C1C	0.0991(8)	0.2528(3)	0.9996(3)	3.2(4)
C2A	0.2693(8)	0.6936(3)	0.2100(3)	2.9(4)	C2C	0.0977(9)	0.2391(4)	1.0519(3)	3.7(5)
C3A	0.3423(9)	0.6364(3)	0.1765(3)	3.5(5)	C3C	-0.0424(9)	0.2131(4)	1.0533(4)	4.2(5)
C4A	0.4820(9)	0.6407(3)	0.2105(3)	3.3(4)	C4C	-0.1199(9)	0.2060(4)	1.0026(4)	4.9(5)
C5A	0.4990(8)	0.7016(3)	0.2484(3)	2.8(4)	C5C	-0.0361(9)	0.2317(4)	0.9710(4)	4.4(5)
C6A	0.1352(9)	0.6377(4)	0.2908(4)	3.9(5)	C6C	0.2165(9)	0.1051(4)	0.9791(4)	4.9(6)
C6A	0.2130(9)	0.5825(3)	0.2574(3)	3.8(5)	C7C	0.073(1)	0.0816(4)	0.9815(4)	5.1(6)
C8A	0.3463(9)	0.5859(3)	0.2854(3)	3.5(5)	C8C	-0.004(1)	0.0728(4)	0.9298(5)	5.9(6)
C9A	0.3443(9)	0.6422(4)	0.3407(3)	3.6(5)	C9C	0.094(1)	0.0872(4)	0.8916(4)	6.4(6)
C10A	0.2143(9)	0.6738(4)	0.3443(3)	3.9(5)	C10C	0.224(1)	0.1072(4)	0.9223(4)	5.7(6)
C11A	0.3487(8)	0.8016(3)	0.2987(3)	3.0(5)	C11C	0.2158(9)	0.2801(3)	0.9772(3)	3.4(5)
C12A	0.4538(9)	0.8499(3)	0.3086(3)	3.3(5)	C12C	0.195(1)	0.3252(4)	0.9537(4)	4.5(5)
C13A	0.3918(9)	0.9055(3)	0.3561(4)	3.5(5)	C13C	0.328(1)	0.3377(4)	0.9330(4)	4.7(6)
C14A	0.2500(9)	0.8933(3)	0.3714(3)	3.3(4)	C14C	0.4375(9)	0.3053(4)	0.9450(4)	4.3(5)
C15A	0.2236(8)	0.8281(3)	0.3361(3)	3.0(4)	C15C	0.367(1)	0.2693(3)	0.9708(4)	4.2(5)
C16A	0.337(1)	0.8892(4)	0.2141(4)	5.0(6)	C16C	0.243(1)	0.4427(4)	1.0784(4)	4.4(5)
C17A	0.274(1)	0.9423(4)	0.2613(4)	4.8(6)	C17C	0.379(1)	0.4521(4)	1.0541(4)	4.3(5)
C18A	0.127(1)	0.9290(4)	0.2737(4)	5.3(6)	C18C	0.488(1)	0.4220(4)	1.0689(4)	4.5(5)
C19A	0.099(1)	0.8668(4)	0.2303(4)	5.7(6)	C19C	0.421(1)	0.3970(4)	1.1059(4)	4.5(5)
C20A	0.227(1)	0.8423(4)	0.1933(4)	5.3(6)	C20C	0.272(1)	0.4089(4)	1.1114(4)	4.5(5)
C21A	0.1125(9)	0.7040(3)	0.2038(4)	3.9(5)	C21C	0.224(1)	0.2449(4)	1.0919(4)	4.6(5)
C22A	0.006(1)	0.6570(4)	0.2019(4)	5.2(6)	C22C	0.261(1)	0.1843(5)	1.0933(4)	6.4(6)
C23A	-0.005(1)	0.6566(4)	0.2727(4)	5.1(6)	C23C	0.319(1)	0.1328(5)	1.0317(6)	7.6(9)
C24A	0.582(1)	0.5859(4)	0.1852(4)	4.8(5)	C24C	-0.262(1)	0.1709(4)	0.9831(5)	7.3(7)
C25A	0.600(1)	0.5678(4)	0.2368(4)	5.7(6)	C25C	-0.259(1)	0.1061(6)	0.9491(7)	12(1)
C26A	0.467(1)	0.5413(4)	0.2565(4)	4.7(6)	C26C	-0.160(1)	0.0590(4)	0.9204(5)	8.2(8)
C27A	0.5917(9)	0.8484(4)	0.2734(4)	4.5(5)	C27C	0.055(1)	0.3599(4)	0.9606(4)	6.0(6)
C28A	0.600(2)	0.8927(7)	0.2429(7)	5(1)	C28C	0.064(1)	0.4287(5)	0.9974(7)	10(1)
C28A'	0.586(3)	0.828(1)	0.207(1)	6.1(6)	C29C	0.098(1)	0.4571(5)	1.0652(5)	7.4(7)
C29A	0.495(1)	0.8794(4)	0.1950(4)	6.2(6)	C30C	0.597(1)	0.3136(4)	0.9400(4)	6.0(6)
C30A	0.141(1)	0.9409(4)	0.4102(4)	4.6(5)	C31C	0.650(1)	0.3810(5)	0.9721(5)	7.7(8)
C31A	0.008(1)	0.9455(4)	0.3763(4)	5.5(6)	C32C	0.642(1)	0.4128(5)	1.0442(4)	6.0(6)
C32A	0.035(1)	0.9701(4)	0.3294(4)	5.8(6)	Fe1D	0.8146(1)	0.34353(5)	0.23519(5)	3.02(6)
Fe1B	0.4583(1)	0.15935(5)	0.47787(5)	3.23(6)	Fe2D	0.7521(2)	0.12956(5)	0.21734(5)	3.88(7)
Fe2B	0.2241(1)	0.36167(5)	0.52100(5)	3.31(7)	C1D	0.8531(8)	0.2665(3)	0.2468(3)	3.1(5)
C1B	0.4405(8)	0.2507(3)	0.5026(3)	2.7(4)	C2D	0.7463(9)	0.3058(3)	0.2896(3)	3.3(5)
C2B	0.4134(8)	0.2376(3)	0.5534(3)	3.1(4)	C3D	0.8154(9)	0.3643(4)	0.3235(3)	3.8(5)
C3B	0.5427(9)	0.2103(3)	0.5601(4)	3.5(4)	C4D	0.9590(9)	0.3635(3)	0.3005(4)	3.6(5)
C4B	0.6432(8)	0.2037(4)	0.5123(4)	3.8(5)	C5D	0.9821(9)	0.3016(3)	0.2533(4)	3.7(5)
C5B	0.5813(8)	0.2310(3)	0.4785(3)	3.4(5)	C6D	0.6266(9)	0.3602(4)	0.2076(4)	4.1(5)
C6B	0.2926(8)	0.1051(4)	0.4750(4)	4.1(5)	C7D	0.7044(9)	0.4162(4)	0.2423(4)	4.0(5)
C7B	0.4244(9)	0.0801(4)	0.4836(4)	4.2(5)	C8D	0.8427(9)	0.4156(3)	0.2152(4)	3.7(5)
C8B	0.5208(9)	0.0705(4)	0.4336(4)	4.5(5)	C9D	0.8471(9)	0.3582(4)	0.1602(4)	3.9(5)
C9B	0.447(1)	0.0867(4)	0.3932(4)	4.8(5)	C10D	0.7160(9)	0.3152(3)	0.1561(3)	3.6(5)
C10B	0.3093(9)	0.1068(4)	0.4181(4)	4.4(5)	C11D	0.8371(9)	0.1996(3)	0.2018(3)	3.3(5)
C11B	0.3407(9)	0.2814(3)	0.4774(3)	3.4(4)	C12D	0.9399(9)	0.1521(4)	0.1896(4)	3.8(5)
C12B	0.3835(9)	0.3273(3)	0.4585(3)	3.6(5)	C13D	0.8809(1)	0.0964(4)	0.1433(4)	4.3(5)
C13B	0.2620(9)	0.3413(4)	0.4333(4)	4.0(5)	C14D	0.7428(9)	0.1070(3)	0.1286(3)	3.7(5)
C14B	0.1393(9)	0.3081(4)	0.4393(3)	3.9(5)	C15D	0.7164(9)	0.1716(3)	0.1637(3)	3.3(5)
C15B	0.1886(9)	0.2698(3)	0.4656(4)	3.6(5)	C16D	0.808(1)	0.1133(4)	0.2868(4)	5.0(6)
C16B	0.3102(9)	0.4416(4)	0.5818(4)	4.1(5)	C17D	0.747(1)	0.0586(4)	0.2384(4)	5.5(6)
C17B	0.187(1)	0.4533(4)	0.5547(4)	4.7(6)	C18D	0.608(1)	0.0713(4)	0.2279(4)	4.7(6)
C18B	0.0652(9)	0.4212(4)	0.5630(4)	4.1(5)	C19D	0.580(1)	0.1341(4)	0.2723(4)	5.2(6)
C19B	0.1070(9)	0.3943(4)	0.6008(4)	4.1(5)	C20D	0.702(1)	0.1596(4)	0.3083(4)	4.8(6)
C20B	0.2564(9)	0.4063(4)	0.6119(3)	4.1(5)	C21D	0.5872(9)	0.2935(4)	0.2948(3)	3.8(5)
C21B	0.2746(9)	0.2419(4)	0.5893(4)	3.9(5)	C22D	0.485(1)	0.3400(4)	0.2893(4)	5.1(6)
C22B	0.221(1)	0.1808(4)	0.5869(4)	5.2(6)	C23D	0.4862(9)	0.3394(4)	0.2264(4)	4.8(6)
C23B	0.1737(9)	0.1310(4)	0.5244(5)	5.5(6)	C24D	1.060(1)	0.4187(4)	0.3170(4)	4.9(5)
C24B	0.781(1)	0.1691(4)	0.4959(4)	5.7(6)	C25D	1.089(1)	0.4372(5)	0.2660(5)	6.6(7)
C25B	0.781(1)	0.1081(5)	0.4457(6)	8.2(8)	C26D	0.963(1)	0.4616(4)	0.2438(4)	5.0(6)
C26B	0.678(1)	0.0563(4)	0.4299(5)	6.5(6)	C27D	1.074(1)	0.1563(4)	0.2251(4)	5.5(6)
C27B	0.528(1)	0.3617(4)	0.4715(4)	4.9(6)	C28D	1.072(1)	0.1196(7)	0.2606(7)	11(1)
C28B	0.521(1)	0.4316(4)	0.5093(5)	6.6(7)	C29D	0.959(1)	0.1224(4)	0.3052(4)	6.8(7)
C29B	0.465(1)	0.4580(4)	0.5751(4)	5.2(6)	C30D	0.633(1)	0.0585(4)	0.0915(4)	5.2(6)
C30B	-0.017(1)	0.3177(4)	0.4294(4)	5.1(6)	C31D	0.497(1)	0.0534(4)	0.1260(4)	5.9(6)
C31B	-0.068(1)	0.3851(5)	0.4640(4)	5.8(6)	C32D	0.517(1)	0.0308(4)	0.1741(5)	6.2(7)
C32B	-0.080(1)	0.4134(4)	0.5340(4)	5.4(6)					

anisotropically. During the final cycles of refinement fixed hydrogen contributions with C–H bond lengths held at 1.08 Å were applied. The final positional parameters for all atoms can be found in Table 2, and the selected bond distances and angles are given in Table 3.

Structure Determination of 17b. A orange crystal (0.43 × 0.18 × 0.19 mm) was obtained by following the same procedure as described for **17a**. Data were collected to a 2θ value of 44.8°. The unit cell dimensions were obtained from 20 reflections with 18.93° < 2θ < 29.55°. Of the 9860 unique reflections, there were 5334 reflections with $F_o > 2.0\sigma(F_o^2)$. These data were used in the final refinement of structural parameters. The structure was solved by the heavy-atom method to locate the Fe positions and successive Fourier maps to reveal the whole molecule and refined

Table 5. Selected Bond Distances (Å) and Bond Angles (deg) for 17b

	independent molecules			
	A	B	C	D
Fe1–C1	2.045(7)	2.016(7)	2.043(7)	2.045(7)
Fe1–C2	2.002(7)	2.000(7)	1.996(8)	2.002(7)
Fe1–C3	1.998(7)	1.999(8)	1.990(8)	1.987(8)
Fe1–C4	1.998(8)	1.986(8)	1.971(9)	1.995(8)
Fe1–C5	2.034(7)	2.034(7)	2.018(9)	2.034(8)
Fe1–C6	1.955(8)	1.964(8)	1.997(9)	1.996(8)
Fe1–C7	1.988(7)	1.996(8)	1.985(8)	1.987(7)
Fe1–C8	2.010(7)	2.008(8)	1.998(9)	2.017(7)
Fe1–C9	2.052(7)	2.028(8)	2.036(9)	2.033(8)
Fe1–C10	2.035(8)	2.002(8)	1.991(8)	2.026(8)
Fe2–C11	2.044(7)	2.052(8)	2.058(8)	2.027(7)
Fe2–C12	1.996(8)	1.987(8)	1.995(8)	1.986(8)
Fe2–C13	1.993(8)	1.997(8)	1.998(8)	1.983(8)
Fe2–C14	1.994(8)	2.002(8)	1.992(8)	1.994(8)
Fe2–C15	2.028(7)	2.035(8)	2.025(8)	2.029(7)
Fe2–C16	1.997(8)	1.994(8)	2.004(8)	1.997(9)
Fe2–C17	2.012(7)	2.015(8)	2.004(8)	2.000(8)
Fe2–C18	2.027(9)	1.985(8)	1.989(8)	2.000(8)
Fe2–C19	2.028(9)	2.029(8)	2.017(8)	2.018(9)
Fe2–C20	2.020(8)	2.018(7)	2.024(8)	2.049(9)
C1–C2	1.45(1)	1.43(1)	1.46(1)	1.43(1)
C1–C5	1.41(1)	1.41(1)	1.42(1)	1.41(1)
C2–C3	1.42(1)	1.43(1)	1.42(1)	1.42(1)
C3–C4	1.43(1)	1.42(1)	1.39(1)	1.42(1)
C4–C5	1.41(1)	1.41(1)	1.40(1)	1.43(1)
C6–C7	1.41(1)	1.43(1)	1.43(1)	1.42(1)
C6–C10	1.42(1)	1.42(1)	1.42(1)	1.41(1)
C7–C8	1.41(1)	1.42(1)	1.40(1)	1.41(1)
C8–C9	1.42(1)	1.42(1)	1.42(1)	1.43(1)
C9–C10	1.42(1)	1.39(1)	1.39(2)	1.41(1)
C11–C12	1.43(1)	1.42(1)	1.46(1)	1.43(1)
C11–C15	1.42(1)	1.44(1)	1.42(1)	1.42(1)
C12–C13	1.44(1)	1.42(1)	1.38(1)	1.42(1)
C13–C14	1.40(1)	1.41(1)	1.41(1)	1.40(1)
C14–C15	1.43(1)	1.43(1)	1.42(1)	1.42(1)
C16–C17	1.41(1)	1.43(1)	1.42(1)	1.43(1)
C16–C20	1.42(1)	1.43(1)	1.42(1)	1.40(1)
C17–C18	1.43(1)	1.40(1)	1.40(1)	1.38(1)
C18–C19	1.42(1)	1.42(1)	1.42(1)	1.44(1)
C19–C20	1.43(1)	1.41(1)	1.40(1)	1.40(1)
C2–C1–C5	107.8(6)	108.9(6)	106.7(7)	108.4(7)
C2–C1–C11	127.1(7)	127.7(7)	129.0(7)	127.9(7)
C5–C1–C11	125.1(6)	123.3(7)	124.3(7)	123.7(7)
C1–C2–C3	106.3(6)	106.1(7)	105.8(7)	106.5(7)
C2–C3–C4	109.1(6)	108.9(7)	109.8(7)	110.0(7)
C3–C4–C5	107.4(6)	107.6(7)	107.8(7)	106.3(7)
C1–C5–C4	109.2(6)	108.3(7)	109.7(7)	108.7(7)
C7–C6–C10	106.8(7)	106.4(7)	103.9(8)	106.1(7)
C6–C7–C8	109.9(7)	107.8(7)	110.6(8)	110.9(7)
C7–C8–C9	106.2(7)	108.0(7)	106.6(8)	105.2(7)
C8–C9–C10	108.7(7)	108.0(8)	107.4(9)	108.9(7)
C6–C10–C9	108.0(7)	109.7(7)	111.3(8)	108.9(7)
C1–C11–C12	123.6(7)	125.2(7)	125.1(7)	126.0(7)
C1–C11–C15	127.5(7)	128.4(7)	130.0(7)	126.5(7)
C12–C11–C15	108.9(6)	106.4(7)	104.8(7)	107.4(6)
C11–C12–C13	105.5(7)	108.6(7)	108.9(7)	106.7(7)
C12–C13–C14	110.1(6)	109.2(7)	109.3(7)	110.2(7)
C13–C14–C15	107.0(6)	106.6(7)	106.7(7)	106.8(7)
C11–C15–C14	108.3(6)	109.1(7)	110.1(7)	108.8(7)
C17–C16–C20	106.7(8)	105.8(7)	106.8(7)	108.3(8)
C16–C17–C18	110.5(8)	109.3(7)	109.1(7)	108.9(8)
C17–C18–C19	105.8(8)	107.4(7)	106.7(8)	106.2(8)
C18–C19–C20	108.7(8)	108.1(7)	109.2(7)	110.0(8)
C16–C20–C19	108.2(7)	109.0(7)	108.0(7)	106.6(6)

with a weighted least-squares routine. Atomic coordinates and selected bond distances and angles are given in Tables 4 and 5, respectively.

Structure Determination of 18a. A black crystal (0.20 × 0.13 × 0.25 mm) was obtained when a layer of hexane was allowed to slowly diffuse into a CH_2Cl_2 solution of **18a**. Data were collected to a 2θ value of 44.9°. The cell dimensions were obtained from 25 reflections with 2θ in the range 14.65–34.40°. Of the 3866

Table 6. Atom Coordinates and Thermal Parameters (Å²) for 18a

	x	y	z	$B_{iso}{}^a$
I1	0.36281(8)	0.77830(7)	0.16700(4)	4.55(4)
I2	0.3787(1)	0.57391(8)	0.20883(5)	5.99(5)
I3	0.3381(1)	0.98030(8)	0.11914(6)	6.63(6)
Fe1	0.9400(2)	0.8024(1)	0.19862(8)	3.00(7)
Fe2	1.2914(2)	0.8331(1)	0.40646(8)	2.84(7)
C1	1.0415(9)	0.8496(7)	0.2937(5)	2.7(5)
C2	0.912(1)	0.8679(8)	0.2847(6)	3.8(6)
C3	0.876(1)	0.9329(8)	0.2223(6)	3.6(6)
C4	0.979(1)	0.9452(7)	0.1929(6)	3.8(6)
C5	1.080(1)	0.8950(8)	0.2370(6)	3.3(5)
C6	0.817(1)	0.6924(9)	0.1846(6)	4.1(6)
C7	0.789(1)	0.761(1)	0.1276(6)	4.5(6)
C8	0.887(1)	0.769(1)	0.0968(6)	4.9(7)
C9	0.979(1)	0.7015(9)	0.1319(6)	4.4(6)
C10	0.937(1)	0.6563(8)	0.1837(6)	4.3(6)
C11	1.1173(9)	0.7906(7)	0.3484(5)	2.4(5)
C12	1.2113(9)	0.7226(8)	0.3394(5)	2.8(5)
C13	1.2725(9)	0.6861(7)	0.4065(5)	2.7(5)
C14	1.218(1)	0.7291(7)	0.4561(5)	2.7(5)
C15	1.1249(9)	0.7975(7)	0.4223(5)	2.8(5)
C16	1.476(1)	0.8470(9)	0.4449(6)	3.9(6)
C17	1.416(1)	0.8831(8)	0.4955(6)	3.5(6)
C18	1.334(1)	0.9606(8)	0.4652(6)	3.7(6)
C19	1.350(1)	0.9742(9)	0.3967(7)	4.9(7)
C20	1.433(1)	0.970(1)	0.3833(6)	4.6(6)
C21	0.827(1)	0.8228(9)	0.3216(6)	3.9(6)
C22	0.718(1)	0.769(1)	0.2741(7)	6.0(8)
C23	0.747(1)	0.676(1)	0.2375(7)	5.3(7)
C24	0.976(1)	0.9928(9)	0.1240(7)	5.1(7)
C25	0.892(2)	0.948(1)	0.0632(9)	9(1)
C26	0.904(2)	0.843(1)	0.0449(6)	6.7(9)
C27	1.387(1)	0.6222(8)	0.4230(6)	4.1(6)
C28	1.496(1)	0.6645(9)	0.4773(6)	4.4(6)
C29	1.552(1)	0.757(1)	0.4514(6)	4.5(7)
C30	1.065(1)	0.8726(9)	0.4577(6)	3.8(6)
C31	1.154(1)	0.9289(9)	0.5177(6)	3.9(6)
C32	1.237(1)	1.0028(9)	0.4948(7)	4.3(6)

^{a} B_{iso} is the mean of the principal axes of the thermal ellipsoid.

unique reflections, there were 2296 reflections with $F_o{}^2 > 2.0\sigma(F_o{}^2)$. These data were used in the final refinement of the structural parameters.

Structure refinement was carried out in the same manner as described for **17a**. The greatest residual electron density upon completion of refinement was in the vicinity of the iodide atoms. Selected bond distances and angles and atomic coordinates are given in Tables 3 and 6, respectively.

Structure Determination of 18b. A black crystal (0.38 × 0.09 × 0.19 mm) was obtained when a layer of ether was allowed to slowly diffuse into a CH_2Cl_2 solution of **18b**. Data were collected to a 2θ value of 49.8°. The cell dimensions were obtained from 25 reflections with 14.72 < 2θ < 31.02. Of the 5197 unique reflections, there were 3727 reflections with $F_o{}^2 > 2.5\sigma(F_o{}^2)$. These data were used in the final refinement of the structural parameters.

Structure refinement was carried out in the same manner as described for **18a**. The greatest residual electron density upon completion of refinement was in the vicinity of the iodide atoms. Selected bond distances and angles and atomic coordinates are given in Tables 3 and 7, respectively.

Results and Discussion

Although the physical properties of **17a** and **17b** are different, it is difficult to assign their structures with certainty solely with NMR spectroscopy. X-ray crystallographic studies of these complexes were undertaken to help elucidate the structures and geometric influences on the rate of intramolecular electron transfer in mixed-valence biferrocenium cations. Before the new physical data are described, a summary of single-crystal X-ray structural results obtained for **17a,b** and **18a,b** will be presented.

Table 7. Atom Coordinates and Thermal Parameters ($Å^2$) for 18b

	x	y	z	$B_{iso}{}^a$
I1	0.77102(3)	0.22273(4)	0.07191(2)	3.91(2)
I2	0.96402(4)	0.07792(4)	0.10834(2)	4.53(2)
I3	0.57734(5)	0.35503(5)	0.02767(3)	6.86(3)
Fe1	0.76711(6)	0.73016(6)	0.14809(3)	2.19(3)
Fe2	0.36933(6)	0.86697(6)	0.20829(3)	2.34(3)
C1	0.6015(4)	0.8074(4)	0.1427(2)	2.3(2)
C2	0.5996(4)	0.6895(4)	0.1309(2)	2.3(2)
C3	0.6690(4)	0.6696(4)	0.0769(2)	2.6(2)
C4	0.7236(4)	0.7693(5)	0.0577(2)	2.8(2)
C5	0.6806(4)	0.8541(4)	0.0981(2)	2.6(2)
C6	0.8140(4)	0.6115(4)	0.2114(2)	2.8(2)
C7	0.8704(4)	0.5966(4)	0.1525(2)	2.8(2)
C8	0.9373(4)	0.6910(5)	0.1370(2)	2.9(2)
C9	0.9278(4)	0.7643(5)	0.1903(2)	3.2(2)
C10	0.8540(5)	0.7153(5)	0.2345(2)	3.1(2)
C11	0.5419(4)	0.8690(4)	0.1917(2)	2.5(2)
C12	0.5182(4)	0.8348(4)	0.2554(2)	2.6(2)
C13	0.4534(4)	0.9188(5)	0.2860(2)	2.9(2)
C14	0.4395(4)	1.0071(4)	0.2414(3)	2.7(2)
C15	0.4900(4)	0.9773(4)	0.1825(2)	2.5(2)
C16	0.2140(4)	0.8276(5)	0.2439(3)	3.6(3)
C17	0.2045(4)	0.9182(5)	0.2008(3)	3.3(3)
C18	0.2493(4)	0.8892(5)	0.1406(3)	3.4(3)
C19	0.2797(5)	0.7753(5)	0.1442(3)	3.9(3)
C20	0.2582(5)	0.7379(5)	0.2068(3)	3.8(3)
C21	0.5435(4)	0.5990(4)	0.1696(3)	3.0(2)
C22	0.6256(5)	0.5072(4)	0.1919(3)	3.5(2)
C23	0.7220(5)	0.5401(5)	0.2388(3)	3.5(2)
C24	0.8179(5)	0.7805(5)	0.0094(2)	3.5(2)
C25	0.9171(5)	0.6975(5)	0.0171(3)	3.6(2)
C26	0.9948(5)	0.7149(5)	0.0752(3)	3.6(3)
C27	0.3955(5)	0.9088(5)	0.3492(3)	3.8(3)
C28	0.2653(6)	0.9167(6)	0.3497(3)	5.1(3)
C29	0.1983(6)	0.8291(6)	0.3141(3)	5.0(3)
C30	0.4737(5)	1.0392(5)	0.1218(3)	3.6(2)
C31	0.3969(6)	0.9858(7)	0.0725(3)	5.9(4)
C32	0.2729(5)	0.9670(6)	0.0875(3)	4.5(3)

^{a} B_{iso} is the mean of the principal axes of the thermal ellipsoid.

A

B

Figure 1. ORTEP drawings for the two independent molecules (A and B) of **17a** with 30% thermal ellipsoids.

Molecular Structure of 17a. The results of our crystallographic study at room temperature show that **17a** crystallizes in the triclinic space group $P\bar{1}$. As shown in Figure 1, there are two crystallographically independent molecules in the unit cell. Collected in Table 3 are selected bond distances and angles. The two independent molecules have very similar geometrical arrangements. However, they do not adopt the usual trans conformation observed in the series of dialkylbiferrocenium cations **1–16**.[7,15] The two Cp rings in the fulvalenide bridge are not coplanar, and the dihedral angles between the two Cp rings of the fulvalenide ligand in the two independent molecules labeled as FeA and FeB are 58.7(2) and 53.6-(2)°, respectively. Inspection of the iron to Cp ligand bond lengths (Fe–Cp) shows that the average distance (1.603(3) Å) is significantly less than the values of 1.65 and 1.70 Å found for ferrocene[30] and ferrocenium,[31] respectively. This is mainly due to the compression of the interannular trimethylene bridge on the Fe atom. The dihedral angles between the two least-squares planes of the Cp rings respectively associated with Fe1A and Fe2A are 9.9(2) and 10.9(2)°, while the two Cp rings in each ferrocenyl moiety are nearly eclipsed with average staggering angles of 0.3(3) and 0.5(3)°. The two Cp rings associated with Fe1B and Fe2B are also nearly eclipsed with average
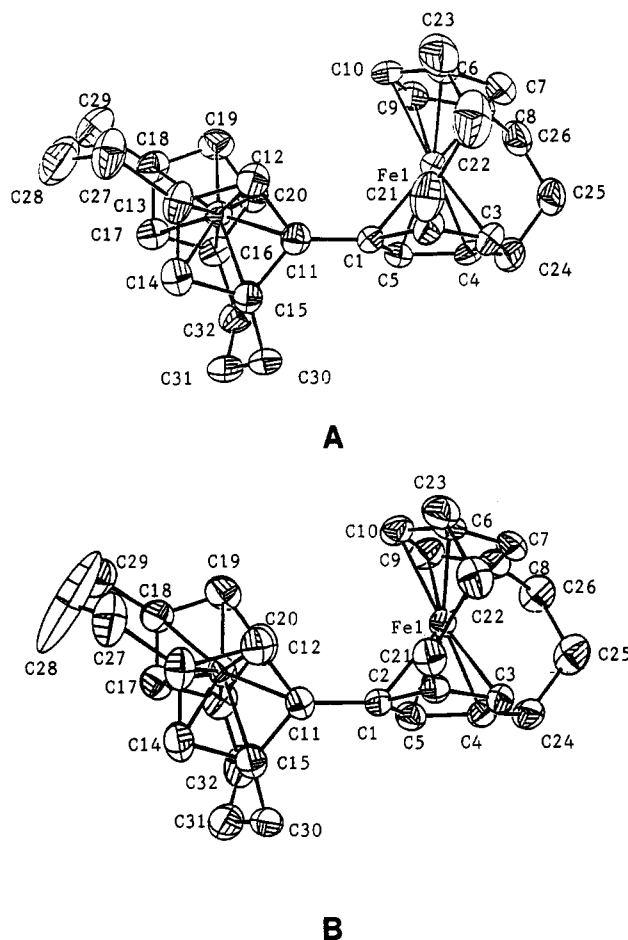
staggering angles of 0.5(3) and 0.4(3)°. Furthermore, the two planes of the Cp rings bonded to Fe1B and Fe2B form dihedral angles of 11.4(2) and 9.0(2)° with the fulvalenide plane, respectively. The average Fe–C bond distance of 2.011(5) Å is less than the values of 2.045 and 2.075 Å found for the ferrocene[30] and ferrocenium ions,[31] respectively. The average C–C bond length (1.426(8) Å) in the Cp rings agrees well with that in ferrocene (1.42 Å).[30]

Molecular Structure of 17b. Compound **17b** crystallizes at room temperature in the triclinic space group $P\bar{1}$. There are four crystallographically independent molecules in the unit cell, and the molecular structures are shown in Figure 2. There is a very similar geometrical arrangement in the four independent molecules. Atomic coordinates and important bond distances and angles are given in Tables 4 and 5, respectively. As found in compound **17a**, compound **17b** also does not adopt the usual trans conformation seen in the series of disubstituted biferrocenium cations **1–16**.[7,15] The dihedral angles between the two least-squares Cp planes of fulvalenide ligands in four independent molecules respectively labeled as A–D in Figure 2 are 53.2(4), 49.1(4), 46.9(4), and 51.4(4)°. The average Fe–Cp and Fe–C bond lengths are 1.606(4) and 2.009(8) Å, respectively. Thus, the average bond distance between the iron atom and the five carbons for a given ring and the average Fe–Cp distance for a ferrocenyl moiety are very similar in both compounds **17a** and **17b**. The two Cp rings in each ferrocenyl moiety are nearly eclipsed with an average staggering angle of 1.4(5)°, while the average dihedral angle between these two Cp rings is 9.9(4)°. The

(30) Seiler, P.; Dunitz, J. D. *Acta Crystallogr., Sect. B* **1979**, *35*, 1068.

(31) Mammano, N. J.; Zalkin, A.; Landers, A.; Rheingold, A. L. *Inorg. Chem.* **1977**, *16*, 297.

(32) Dong, T.-Y.; Hwang, M. Y.; Wen, Y. S. *J. Organomet. Chem.* **1990**, *391*, 377.
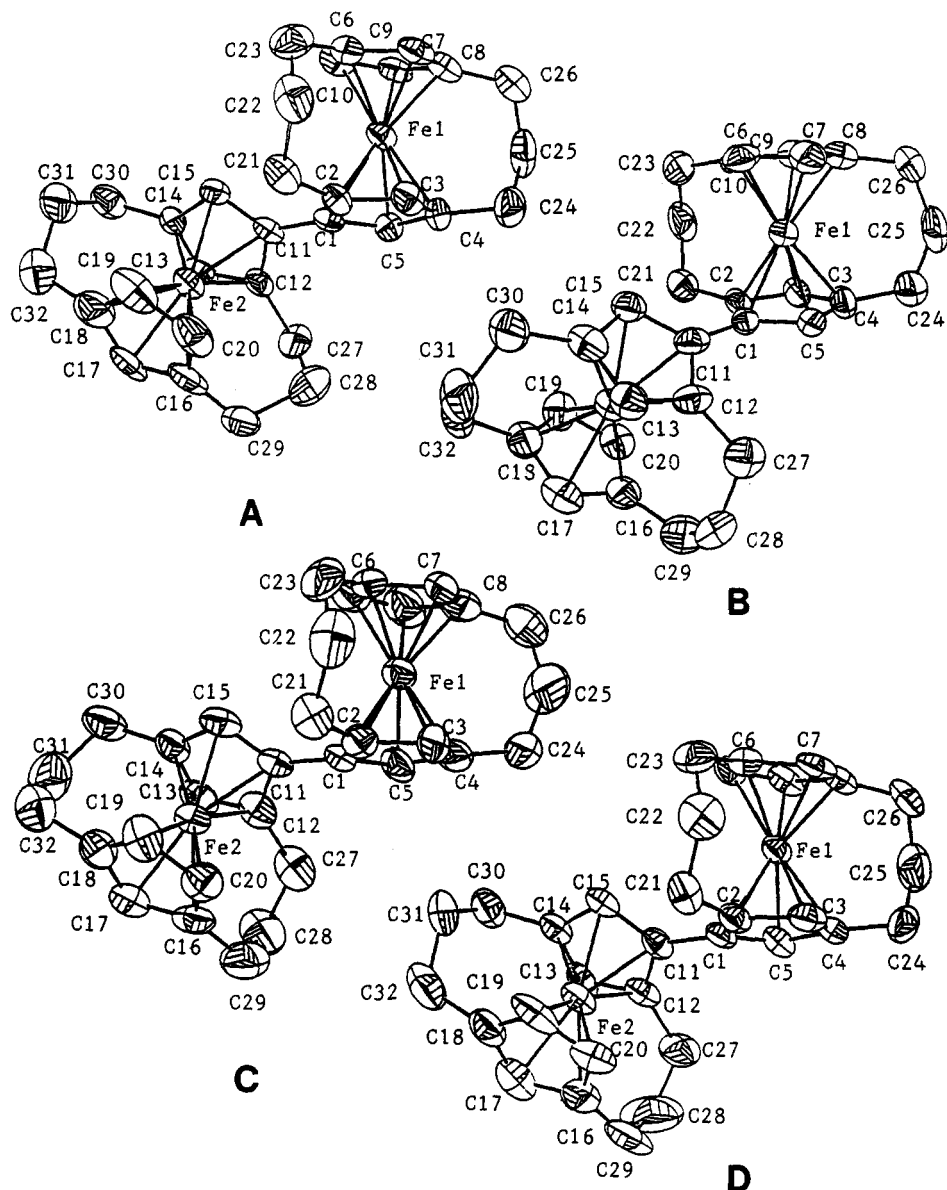
Figure 2. ORTEP drawings for the four independent molecules (A–D) of **17b** with 30% thermal ellipsoids.

average C–C bond length (1.42(1) Å) in the Cp rings also agrees well with that in ferrocene (1.42 Å).[30]

Molecular Structure of 18a. A drawing of the mixed-valence compound **18a** is shown in Figure 3. Important bond distances and angles are collected in Table 3. The two metallocene moieties in the cation are not equivalent. In comparison with ferrocenes[30] and **17a**, the average Fe1–Cp distance (1.608(6) Å) and the average Fe1–C interatomic distance (2.02(1) Å) indicate that the Fe1(Cp)$_2$ metallocene unit is in the Fe(II) oxidation state. However, the average Fe2–Cp distance (1.658(6) Å) and the average Fe2–C distance (2.06(1) Å), which are larger than the corresponding values in **17a**, indicate that the Fe2(Cp)$_2$ unit is the Fe(III) metallocene moiety. Such an increase in Fe–Cp and Fe–C distances has been observed when ferrocenes are oxidized to the corresponding ferrocenium cations.[18,31] There is no significant difference for C–C bond distances in the Cp rings between two nonequivalent Fe(II) and Fe(III) metallocene moieties. The observation of two nonequivalent Fe(II) and Fe(III) moieties is consistent with our Mössbauer studies.

The conformational relationship between two iron metallocene moieties plays an important role in determin-ing the magnitude of electron-transfer rate. As can be seen in Figure 3, the two metallocene units are twisted relative to each other. The dihedral angle between the two Cp rings in the fulvalenide ligand is 42.0(5)°. The two Cp rings associated with Fe1 are not quite parallel, with a dihedral angle of 11.2(5)°. The dihedral angle between the two Cp rings associated with Fe2 is 14.6(5)°. Furthermore, the two Cp rings associated with Fe1 and Fe2 are nearly eclipsed with average angles of 0.8(7) and 2.1(7)°, respectively.

The triiodide anion in **18a** is essentially linear, and the I2–I1–I3 angle is 177.26(4)°. The triiodide anion also shows an essentially symmetric structure. The distance from I1 to I2 is 2.905(2) Å, while the distance from I1 to I3 is 2.908(2) Å.

Molecular Structure of 18b. The results of our crystallographic study at room temperature show that **18b** crystallizes in the monoclinic space group $P2_1/n$, and the molecular structure is shown in Figure 4. Collected in Table 3 are selected bond distances and angles. The two metallocene moieties in the cation are not equivalent. In comparison with **17b**, the average Fe1–Cp distance (1.662-(2) Å) and the average Fe1–C distance (2.059(5) Å) indicate
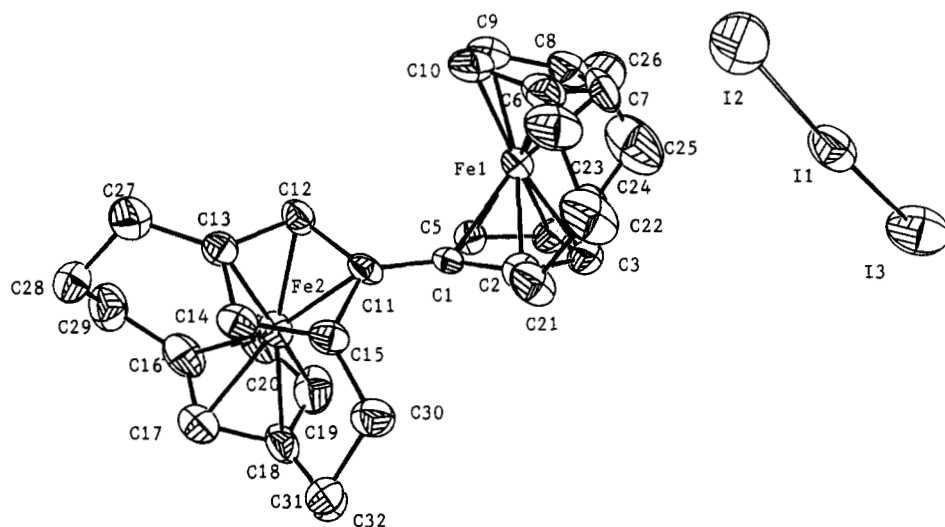
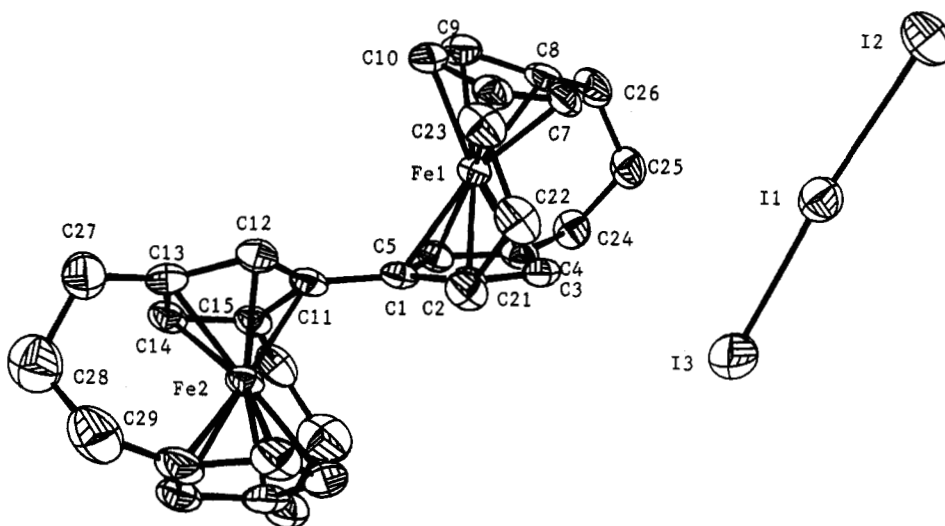**Figure 3.** ORTEP drawing for **18a** with 30% thermal ellipsoids.

Figure 4. ORTEP drawing for **18b** with 30% thermal ellipsoids.

that this metallocene is in the Fe(III) oxidation state. The average Fe2–Cp distance (1.608(2) Å) and the average Fe2–C distance (2.016(5) Å) indicate that this metallocene is in the Fe(II) oxidation state. The observation of two nonequivalent Fe(II) and Fe(III) moieties is also consistent with our Mössbauer studies.

Similar to the geometrical arrangement for **18a**, in **18b** the two metallocene units are also twisted relative to each other. The dihedral angle between the two Cp rings in the fulvalenide ligand is 38.80(22)°. The two Cp rings respectively associated with Fe1 and Fe2 are not quite parallel, with dihedral angles of 19.25(23) and 9.74(24)°. Furthermore, the two Cp rings associated with Fe1 and Fe2 are nearly eclipsed with average staggering angles of 0.4 and 1.6(4)°, respectively.

The triiodide anion in **18b** is slightly asymmetric (I1–I2 = 2.9393(6) Å and I1–I3 = 2.9058(7) Å). The angle I2–I1–I3 is 175.65(2)°.

Electrochemical Results. Electrochemical data for compounds **17a,b**, as well as those for some other relevant compounds, are shown in Table 8. The neutral compounds **17a,b** undergo two successive reversible one-electron oxidations to yield the mono- and then the dication. Electrochemical reversibility was demonstrated by the peak-to-peak separation between the resolved reduction and oxidation wave maxima.

Table 8. Electrochemical Data for Various Biferrocenes

| compd	$E_{1/2}$ (V)[a]	$\Delta E_{1/2}$ (V)[b]	Δ (mV)[c]	$10^{-5}K_{com}$
ferrocene	0.37		70	
biferrocene	0.28	0.31	70	1.80
	0.59		75	
17a	0.244	0.333	66	4.41
	0.577		65	
17b	0.246	0.326	65	3.35
	0.572		74	

[a] All half-wave potentials are referred to the Ag⁺/Ag electrode. [b] Peak separation between two waves. [c] Peak-to-peak separation between the resolved reduction and oxidation wave maxima.

In the case of biferrocenes, there are two possible types of interactions between the two ferrocene moieties: interaction propagated through the fulvalenide and through space (electric field effect).[22] It is reasonable to believe that the interaction through the fulvalenide between two Fe sites is strongly favored. Furthermore, it has been shown that the magnitude of the peak-to-peak separation ($\Delta E_{1/2}$) gives an indication of the interaction between the two Fe sites.[33] A comparison of the magnitude of $\Delta E_{1/2}$ for **17a** (0.333 V) with that for **17b** (0.326 V) indicates that the magnitude of interaction between the two Fe sites in

(33) Morrison, W. H., Jr.; Krogsrud, S.; Hendrickson, D. N. *Inorg. Chem.* **1973**, *12*, 1998.

17a is similar to that in 17b. However, a comparison of $\Delta E_{1/2}$ values for 17a,b with that for biferrocene indicates that the interaction between the two Fe sites in 17a,b is larger than that in biferrocene. As reported before,[22,33] the conformational relationship between the two Cp rings in the fulvalenide bridge is critical to the magnitude of Fe–Fe interactions in biferrocene compounds. In contrast to 17a,b, the two Cp rings of the fulvalenide bridge in biferrocene are crystallographically coplanar.[34] Hence, it appears that in the solution state the two Cp rings of the fulvalenide bridge in 17a,b have to be coplanar in order to have a larger Fe–Fe interaction. This is different from the solid-state structures of 17a,b.

Coulometry experiments show that each of the two waves is a one-electron-transfer process. In eq 1 the abbreviation

$$[2,2] + [3,3] \overset{K}{\rightleftharpoons} 2[2,3] \qquad (1)$$
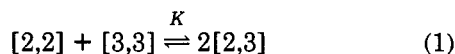
[3,3] denotes the dioxidized salt, [2,3] the monooxidized salt, and [2,2] the neutral compound. Comproportionation equilibrium constants K for 17a,b are 4.41×10^5 and 3.35×10^5, respectively. Quantitative calculations based on the concentration of [2,3] have been corrected for this equilibrium.

Electron Transfer in the Solution State. A description of the width of the intervalence transition band (IT band), the extent of electron delocalization, and the electron-transfer properties of mixed-valence dimers has been given by Hush.[35] Hush has derived an expression for the bandwidth (in cm^{-1}) at half-maximum of the IT band of a localized homonuclear mixed-valence dimer at 300 K as shown in eq 2, where ν_{max} is the frequency in cm^{-1}

$$\Delta\nu_{1/2} = 2310\nu_{max} \qquad (2)$$

$$\Delta E^* = {}^1/_4\nu_{max} \qquad (3)$$

$$\alpha^2 = (4.24 \times 10^{-4})\epsilon_{max}(\Delta\nu_{1/2})/\nu_{max}d^2 \qquad (4)$$

$$H_{ab} = \nu_{max}\alpha \qquad (5)$$

$$K_{et} = \nu_{et} \exp(-\nu_{max}/4K_BT) \qquad (6)$$

$$\nu_{et} = (2\pi/\hbar)H_{ab}{}^2(\pi/K_BT\nu_{max})^{1/2}$$

of the absorption maximum. For a system with harmonic nuclear motion, the energy of activation ΔE^* is related to the energy of the IT band maximum (ν_{max}) as shown by eq 3 for the weak-electron-exchange coupling case. The magnitude of the delocalization can be obtained by a calculation of the delocalization parameter α^2 and electronic coupling H_{ab} from eqs 4 and 5. In eqs 4 and 5 ϵ_{max} is the extinction coefficient and d is the donor–acceptor distance. The average value (5.1 Å) of Fe–Fe distances in a series of dialkyl mixed-valence biferrocenium cations is used as the donor–acceptor distance.[7,15] Finally, the rate constant (K_{et}) of intramolecular electron transfer can be estimated from eq 6, where ν_{et} is the hopping frequency.

In common with most mixed-valence complexes, the mixed-valence compounds 18a,b in CH_2Cl_2 have an IT band at 5050 and 4808 cm^{-1}, respectively, which is not present for the neutral compound or dioxidized ion. The

(34) Kaluski, Z. L.; Struchkov, Yu. T.; Avoyan, R. L. *Zh. Strukt. Khim.* 1964, 5, 743.
(35) Hush, N. S. *Prog. Inorg. Chem.* 1967, 8, 391.

Table 9. Absorption Maxima of IT Bands and Activation Parameters

compd	$\nu_{max}{}^a$	$\epsilon_{max}{}^b$	$\Delta\nu_{1/2}$ (obsd)^a	$\Delta\nu_{1/2}$ (calcd)^a	α^2	H_{ab}	$10^{-12}K_{et}$
1	4762	980	3670	3240	0.0123	528	1.96
16	4762	2880	2898	3317	0.0286	805	4.68
18a	5050	2690	2170	3415	0.0188	692	2.31
18b	4808	2930	2150	3333	0.0214	703	3.26

^{a} In cm^{-1}. ^{b} In M^{-1} cm^{-1}.

absorption maximum and activation parameters calculated from eqs 2–6 were collected in Table 9, together with those for other relevant compounds. An interesting finding is that the IT bands of interannular trimethylene-bridged biferrocenium cations 16 and 18a,b are all sharper than what is expected on the basis of eq 2. An agreement, to about 10%, between $\Delta\nu_{1/2}$(calcd) and $\Delta\nu_{1/2}$(obsd) is usually taken as an indication that the Hush model is a satisfactory description of a localized mixed-valence system. In the case of 1, a good agreement is observed. A sharper band is usually observed for a delocalized mixed-valence compound. For example, the IT band in the Creutz–Taube ion is about 6 times sharper than that predicted by eq 2.[36] The Hush model is derived for the high-temperature limit, the criterion for that limit being $2RT > h\nu$, where $h\nu$ is the energy associated with a metal–ligand vibrational transition. For either a Fe(II)– or a Fe(III)–Cp vibration in 16 and 18a,b, at room temperature we are not at the high-temperature limit. Owing to the interannular trimethylene bridge, the Fe–Cp vibrational energy in 16 and 18a,b is higher than that in 1. Possibly as a consequence of this fact, Hush's correlation of band energy with band width (at room temperature; eq 2) fails.

The extent of delocalization of the exchanging electron in mixed-valence cations can be estimated from the properties of their IT bands. A measure of delocalization in both the ground and excited states is α^2, which can be calculated from eq 4. The experimental α^2 value is the average of α^2 values for the ground and excited states. If delocalization is small, the electronic wave functions used for overlap are relatively unperturbed, and α^2 is a direct measure of delocalization in the ground state. As shown in Table 9, in all cases there is good evidence for localized valences and delocalization from Fe(II) to Fe(III) is less than 3%.

From the rate constants illustrated in Table 9, the electron-transfer rates in 16 and 18a,b are faster than that in biferrocenium triiodide (1). This difference in rate clearly indicates that the interannular bridge also plays an important role in controlling the rate of electron transfer.

^{57}Fe Mössbauer Characteristics. Variable-temperature Mössbauer spectra were run for compounds 18a,b. The various absorption peaks in each spectrum were fitted to Lorentzian lines, and the resulting fitting parameters are summarized in Table 10. The variable-temperature Mössbauer spectra for 18a are shown in Figure 5. The features in these spectra include two doublets which have the same area, as deduced by a least-squares fitting. This pattern of two doublets is expected for a mixed-valence biferrocenium cation which is valence-trapped on the time scale of the Mössbauer technique (electron-transfer rate less than $\sim 10^7$ s^{-1}). The valence-trapped electronic structure is also observed for compound 18b. As illustrated

(36) Creutz, C.; Taube, H. *J. Am. Chem. Soc.* 1973, 95, 1086.

Table 10. ^{57}Fe Mössbauer Least-Squares-Fitting Parameters

compd	T (K)	ΔE_Q (mm/s)[a]	δ (mm/s)[b]	Γ (mm/s)[c]
1	300	1.908	0.486	0.260, 0.276
		0.386	0.487	0.282, 0.292
18a	300	1.864	0.356	0.259, 0.284
		1.273	0.368	0.285, 0.302
	200	1.869	0.401	0.253, 0.265
		1.334	0.411	0.274, 0.295
	150	1.874	0.416	0.246, 0.255
		1.357	0.428	0.280, 0.291
	77	1.878	0.434	0.253, 0.254
		1.371	0.448	0.285, 0.289
18b	300	1.766	0.370	0.357, 0.379
		1.079	0.382	0.438, 0.438
	77	1.825	0.437	0.328, 0.342
		1.146	0.456	0.442, 0.431
19	300	0.148	0.382	0.314, 0.472
20	300	0.541	0.321	0.298, 0.332
	77	0.556	0.404	0.568, 1.168
21	300	0.936	0.425	0.341, 0.312
	77	1.023	0.514	0.285, 0.274
22	300	0.627	0.256	0.282, 0.309
	77	0.738	0.347	0.382, 0.533
23	300	2.111	0.434	0.225, 0.229
		0.771	0.418	0.265, 0.295
	77	2.137	0.521	0.239, 0.245
		0.841	0.514	0.284, 0.291

[a] Quadrupole splitting. [b] Isomer shift. [c] Full width at half-height taken from the least-squares fitting program. The width for the line at more positive velocity is listed first for the doublet.
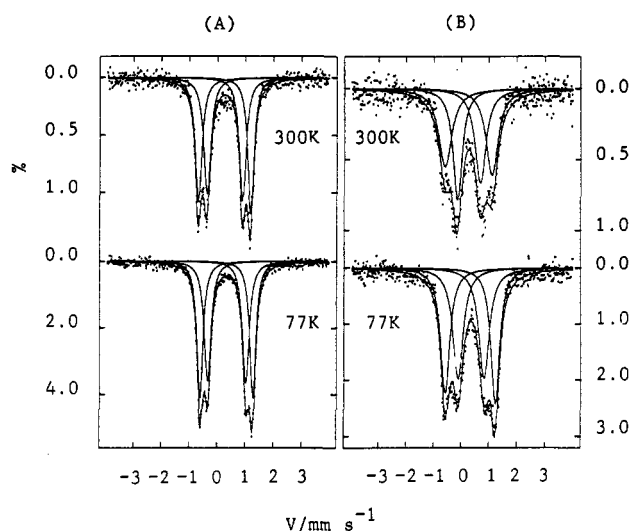

Figure 5. ^{57}Fe Mössbauer spectra for **18a** (A) and **18b** (B).

in Figure 5, the features in the 300 K spectrum of **18b** are two doublets, one with a quadrupole splitting (ΔE_Q) of 1.177 mm s^{-1} (Fe(III) site) and the other with ΔE_Q = 1.826 mm s^{-1} (Fe(II) site). Furthermore, both doublets have the same area by a least-squares fitting to Lorentzian line shapes.

As mentioned in the Introduction, compound **16** has a delocalized electronic structure above 77 K (electron-transfer rate greater than $\sim$10^7 s^{-1}).[21,24] Thus, there is a dramatic difference in electron-transfer rates between **16** and **18**. We believe that this is mainly due to the differences in coplanarity of the two Cp rings in the fulvalenide ligand in **16** and **18**. The single-crystal X-ray determinations of **18a,b** indicate that the π interaction between the two ferrocenyl moieties is destroyed as the linking bond of the two ferrocenyl units is twisted.

The Mössbauer results also lead us to conclude that compound **16** has a localized electronic ground state at 4.2 K (electron-transfer rate <10^{7}s^{-1}). However, it is necessary

Chart 2
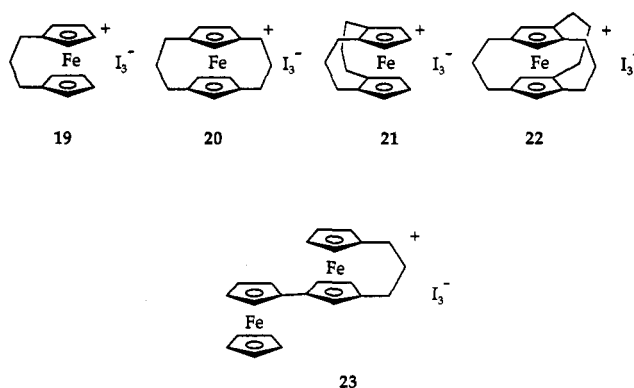
to discuss why the ferrocenium moiety in **16** and **18a,b** has an unusually large quadrupole splitting of $\sim$1.3 mm s^{-1}. In general, ferrocenyl groups (electronic ground state $^1A_{1g}$) give spectra characterized by large quadrupole splitting in the range of 2.0–2.2 mm s^{-1}, while the spectra of ferrocenium cations (electronic ground state $^2E_{2g}$) are characterized by small or vanishing quadrupole splitting.[37] In the case of a Mössbauer localized mixed-valence biferrocenium cation, the value of ΔE_Q in the ferrocenyl moiety is slightly smaller than what is expected for a Fe-(II) ferrocenyl unit and the Fe(III) ferrocenium moiety has a slightly larger ΔE_Q value. Of course, this is a reflection of the admixture of Fe(II) and Fe(III) moieties into the ground state.[7,37] For instance, compound **1** gives a 300 K Mössbauer spectrum with two doublets (ΔE_Q = 1.908 and 0.386 mm s^{-1}).[7] Temperature-dependent Mössbauer delocalized mixed-valence biferrocenium cations (for example, compound **2**) at temperatures below transition temperature show two doublets, one for Fe(II) and the other for Fe(III) sites.[7,8] Increasing the temperature causes the two doublets to move together and eventually to become a single average-valence doublet ($\Delta E_Q \approx$ 1.1 mm s^{-1}) at transition temperature. In our case, the unusually large ΔE_Q value cannot be explained in terms of an admixture of Fe(II) and Fe(III) electronic descriptions. For compounds **18a,b**, as the temperature of the sample is increased from 77 to 300 K, it is interesting to find that the two doublets do not move together. To explain this unusual observation, we have prepared the series of model compounds **19–23** to understand the influence of an interannular trimethylene bridge on the electronic ground state of the ferrocenium cation (Chart 2). Surprisingly, a large quadrupole splitting is observed in the Mössbauer spectra of **20–22** at 300 K. The ΔE_Q values of **19–22** are 0.148, 0.541, 0.936, and 0.627 mm s^{-1}, respectively. For the asymmetric mixed-valence compound **23**, the features in the 300 K Mössbauer spectrum are two doublets, one for the Fe(II) metallocene (ΔE_Q = 2.111 mm s^{-1}) and the other for the Fe(III) metallocene (ΔE_Q = 0.771 mm s^{-1}).[38] The Mössbauer studies clearly indicate that the electronic ground state of the Fe(III) metallocene in **19–23** is not a pure $^2E_{2g}$ state. In compounds **19–23**, the Cp rings are tilted from the parallel geometry for ferrocenium. Bending back the Cp rings leads to an increase of $d_{x^2-y^2}$,d_{xy}-ring overlap. In other words, the metal nonbonding orbitals start to interact with the ligand π orbitals. Under these circumstances the iron ions lose some degree of their Fe-

(37) Morrison, W. H., Jr.; Hendrickson, D. N. *Inorg. Chem.* **1975**, *14*, 2331.

(38) Dong, T.-Y.; Lin, H. M. *J. Organomet. Chem.* **1992**, *426*, 369.

(III) character, and this results in an increase in ΔE_Q because each iron ion is closer to Fe(II) in its properties. This is what we observe for compounds **16**, **18a,b**, and **19–23**.

Conclusions and Comments

Mössbauer spectra indicating the presence of localized electronic structure have been observed for **18a,b**. The energy and the line shape of the IT band clearly indicate that the intramolecular electron-transfer rates in **18a** and **18b** in solution are greater than in the solid state. In the solid state, the rate of electron transfer for a given mixed-valence cation is influenced by various structural factors and lattice dynamics,[6,7] including the electronic and vibronic couplings between two metal ions, the nature of the counterion, and cation–anion interactions.[11,12] In general, the electron-transfer rate for a given mixed-valence biferrocenium cation in the solution state is greater than that in the solid state. In the solid state, we have demonstrated that relatively minor perturbations caused by interactions between neighboring cations and anions have pronounced effects on the electron transfer.[18] In solution, the manner in which the mixed-valence cation is solvated also influences the rate of intramolecular electron transfer. If ion pairing is present, the anion must move rapidly so as not to limit the rate of intramolecular electron transfer. However, in the case of **18a,b**, we believe that the most important factor determining the difference of intramolecular electron-transfer rate between the solution and the solid state is the degree of coplanarity between two Cp rings in the fulvalenide bridge. As is evident in the section Electrochemical Results, in the solution state the two Cp rings of the fulvalenide bridge in the cations of **17a,b** are coplanar. However, the two Cp rings of the fulvalenide bridge in **18a,b** are not crystallographically coplanar.

We have also demonstrated that the perturbations caused by interannular trimethylene bridges have dramatic influences on the electronic structure in a series of model compounds. The cation in each of compounds **18–23** serves as a very sensitive probe of the microscopic structure of the electronic state. Characterization of the electronic ground state in these cations by magnetic susceptibility and EPR and an investigation of the counterion effects on the rate of electron transfer in the solid state are underway. Calculations of the theoretical values of ΔE_Q in the cations of **18–23** are also in progress.

Supplementary Material Available: Complete tables of positional parameters, bond lengths and angles, and thermal parameters for **17a,b** and **18a,b** (48 pages). Ordering information is given on any current masthead page.

OM940127V